

# Analysis of ring-structured Bragg fibres for single TE mode guidance

Alexander Argyros<sup>1,2</sup>, Ian M. Bassett<sup>1</sup>,  
Martijn A. van Eijkelenborg<sup>1</sup>, Maryanne C. J. Large<sup>1</sup>

<sup>1</sup>Australian Photonics Cooperative Research Centre, Optical Fibre Technology Centre, University of Sydney, 206 National Innovation Centre, Australian Technology Park, Eveleigh, NSW 1430, Australia.

<sup>2</sup>School of Physics, University of Sydney, NSW 2006, Australia  
[a.argyros@ofc.usyd.edu.au](mailto:a.argyros@ofc.usyd.edu.au)

<http://www.ofc.usyd.edu.au>

**Abstract:** Ring-structured Bragg fibres that support a single TE-polarisation mode are investigated. The fibre designs consist of a hollow core and rings of holes concentric with the core, which form the low-index layers of the Bragg reflector in the cladding. The effects of varying the air fraction in each ring of holes on the transmission properties of the fibres are analysed and an approximate model based on homogenisation is explored. Surface modes and transitions thereof are also discussed.

©2004 Optical Society of America

**OCIS codes:** (060.2430) Fibers, single-mode; (230.1480) Bragg Reflectors; (060.2280) Fibre design and fabrication; (230.5440) Polarization-sensitive devices; (260.5430) Polarization

---

## References and Links

1. P. Russell, "Photonic crystal fibers," *Science* **299**, 358-62 (2003).
2. T. A. Birks, J.C. Knight, P. St. J. Russell, "Endlessly single-mode photonic crystal fiber," *Opt. Lett.* **22**, 961-3 (1997).
3. R. F. Cregan, B. J. Managan, J. C. Knight, T. A. Birks, P. St. J. Russell, P. J. Roberts, D. C. Allen, "Single-mode photonic band gap guidance of light in air," *Science* **285**, 1537-9 (1999).
4. S. G. Johnson, M. Ibanescu, M. Skorobogatiy, O. Weisberg, T. D. Engeness, M. Soljacic, S. A. Jacobs, J. D. Joannopoulos, Y. Fink, "Low-loss asymptotically single-mode propagation in large-core OmniGuide fibers," *Opt. Express* **9**, 748-79 (2001), <http://www.opticsexpress.org/abstract.cfm?URI=OPEX-9-13-748>.
5. B. Temelkuran, S. D. Hart, G. Benoit, J. D. Joannopoulos, Y. Fink, "Wavelength-scalable hollow optical fibres with large photonic bandgaps for CO<sub>2</sub> laser transmission," *Nature* **420**, 650-3 (2002).
6. A. Argyros, I. M. Bassett, M. A. van Eijkelenborg, M. C. J. large, J. Zagari, N. A. P. Nicorovici, R. C. McPhedran, C. M. de Sterke, "Ring structures in microstructured polymer optical fibres," *Opt. Express* **9**, 813-20 (2001), <http://www.opticsexpress.org/abstract.cfm?URI=OPEX-9-13-813>.
7. A. Argyros, N.A. Issa, I. Bassett, M. A. van Eijkelenborg, "Microstructured optical fiber for single-polarization air guidance," *Opt. Lett.* **29**, 20-2 (2004).
8. G. Vienne, Y. Xu, H. J. Deyerl, T. P. Hansen, B. H. Larsen, J. B. Jensen, T. Sorensen, M. Terrel, Y. Huang, R. Lee, N. A. Mortensen, J. Broeng, H. Simonsen, A. Bjarklev, A. Yariv, "First demonstration of air-silica Bragg fiber," *Optical Fiber Communication Conference & Exposition Postdeadline Papers (Institute of Electrical and Electronics Engineers, New York, 2004)*, PDP25.
9. I. Bassett, A. Argyros, "Elimination of polarization degeneracy in round waveguides," *Opt. Express* **10**, 1342-6 (2002), <http://www.opticsexpress.org/abstract.cfm?URI=OPEX-10-23-1342>.
10. A. Argyros, "Guided modes and loss in Bragg fibres," *Opt. Express* **10**, 1411-7 (2002), <http://www.opticsexpress.org/abstract.cfm?URI=OPEX-10-24-1411>.
11. J. Noda, K. Okamoto, Y. Sasaki, "Polarization maintaining fibers and their applications," *J. Lightwave Technol.* **4**, 1071-89 (1986).
12. A. Ferrando, J. J. Miret, "Single-polarization single-mode intraband guidance in supersquare photonic crystals fibers," *App. Phys. Lett.* **78**, 3184-6 (2001).
13. N.A. Issa, L. Poladian, "Vector wave expansion method for leaky modes of microstructured optical fibres," *J. Lightwave Technol.* **21**, 1005-12 (2003).
14. K. Sakoda, *Optical Properties of Photonic Crystals*, Chapter 2 (Springer-Verlag, Berlin, 2001).
15. H. A. McLeod, *Thin-film optical filters*, Chapter 5 (Adam Hilger Ltd, London, 1969).
16. Y. Xu, A. Yariv, J. G. Fleming, S.-Y. Lin, "Asymptotic analysis of silicon based Bragg fibers," *Opt. Express* **11**, 1039-49 (2003), <http://www.opticsexpress.org/abstract.cfm?URI=OPEX-11-9-1039>.

17. S. E. Golowich, M. I. Weinstein, "Homogenisation expansion for resonances of microstructured photonic waveguides," *J. Opt. Soc. Am. B* **20**, 633-47 (2003).
  18. V. Rastogi, K. S. Chiang, "Holey optical fiber with circularly distributed holes analyzed by the radial effective-index method," *Opt. Lett.* **28**, 2449-51 (2003).
  19. The example used for comparison in Ref. [14] was re-modelled using the same method as for the rest of the calculations presented here. This method is more accurate than that used for the original comparison, and yielded the agreement quoted here, which differs from the original in [14].
  20. G.W. Milton, *The theory of composites*, (Cambridge University Press, London, 2001).
  21. A.W. Snyder, J.D. Love, *Optical Waveguide Theory*, Chapter 30 (Chapman and Hall, New York, 1983).
  22. K. Saitoh, N. A. Mortensen, M. Koshiba, "Air-core photonic band-gap fibers: the impact of surface modes," *Opt. Express* **12**, 394-400 (2004) <http://www.opticsexpress.org/abstract.cfm?URI=OPEX-12-3-394>.
- 

## 1. Introduction

Many properties not available to conventional optical fibres have been shown to be possible with microstructured optical fibres [1]. Such properties include single-mode operation over a large wavelength range [2] and guidance in an air core using photonic band gap fibres [3] or Bragg fibres [4,5]. In microstructured fibres arrangements of holes spanning the entire length of the fibre are used to confine the light. The holes can reduce the refractive index of the region surrounding a high-index core and confine the light by total internal reflection, or, if the holes form a 2D lattice, they confine the light by means of a photonic band gap. Bragg fibres use a 1D photonic band gap formed by layers of alternating high-low refractive index surrounding the core. Ring-structured Bragg fibres have also been proposed [6,7], in which rings of holes form the low index layers of the Bragg reflector in the cladding. Such fibres, with a hollow core, have been demonstrated recently using silica [8].

Previously, designs were proposed for a Bragg fibre [9,10] and a ring-structured Bragg fibre [7] that would support a single TE mode. The advantage gained by this, in comparison to guiding only a  $HE_{11}$  mode as in other cases, is that the TE modes are not polarisation degenerate. The single-TE-mode property would remove polarisation mode dispersion and polarisation fading in interferometers as well as orientation issues (being, for most purposes, circularly symmetric) associated with other single-polarisation fibres [11,12], all of which isolate linear polarisations. A single TE mode was isolated by choosing the angle required for Bragg reflection close to the Brewster angle, meaning that a band gap only formed for the TE polarisation.

The ring-structured fibre design with the single-TE-mode property consists of a hollow core surrounded by circular rings of holes concentric with the core, embedded in a host material of homogeneous refractive index. It has been shown [7] that increasing the number of rings of holes in such a structure resulted in a dramatic decrease in the confinement loss of the  $TE_{01}$  mode, whilst the remaining modes remained largely unaffected with very high confinement loss. This would effectively render these modes unguided, isolating the  $TE_{01}$  mode as the only guided mode.

In this paper the effect of another parameter of that design is investigated: the air fraction of each ring of holes, determined by the number of holes in each ring. Intuitively, lowering the air fraction would serve to raise the "average" refractive index of each ring, without defining this term at present. How the number of holes per ring affects the low-loss TE mode and the high loss modes is examined and effects related to Brewster angle reflections are observed. This work contributes to a better understanding of how the ring-structured Bragg fibres work.

Of particular interest is the possibility of approximating each microstructured Bragg fibre with an equivalent conventional Bragg fibre design. This involves replacing each ring of holes with a homogeneous low index layer, the refractive index profile of which would be determined by the air fraction of each ring of holes of the original ring-structured design. The advantage sought through this process is the ability to model the microstructured designs as

circularly symmetric ones to greatly increase the speed and efficiency of numerical simulations, and thus allow for a larger parameter space to be explored more easily when designing or optimising such fibres.

Finally, the surface modes (modes supported in the solid part of the microstructure, rather than the hollow core) of the microstructured Bragg fibres are examined and shown to present interesting dispersion properties near the avoided crossings with the hollow core modes. These modes were observed to undergo certain transitions that are discussed.

## 2. Fibre designs and numerical simulations

The fibre designs analysed here consist of a hollow core of radius  $r_{co} = 2.4795 \mu\text{m}$ , surrounded by rings of holes with  $\Lambda_e = 0.578 \mu\text{m}$  signifying the external pitch, i.e. the spacing between the centres of holes in adjacent rings, and  $\Lambda_i$  the internal pitch, i.e. the spacing between the centres of adjacent holes in the same ring. The diameter of the holes is given by  $d = 0.335 \mu\text{m}$  and the refractive index of the host material by  $n_1 = 1.49$  corresponding to polymethylmethacrylate, as used in [6] (see Fig. 1). The parameter of interest in this work is the air fraction  $f$  of each ring, asymptotically given by  $f = \pi d / (4\Lambda_i)$ . The values of  $\Lambda_i$  considered were  $0.403, 0.454, 0.519$  and  $0.607 \mu\text{m}$ , giving  $f = 0.65, 0.58, 0.51$  and  $0.43$  respectively. The maximum air fraction for these designs is  $d/4 = 0.78$  and is set by the assumption of circular holes. If annular sectors rather than circular holes were used, as in [8], an air fraction approaching 1.0 would be possible.

For each value of the air fraction the number of rings was varied from 1, 2, 3, 6, 9. The specific values of the various parameters were based upon previous fibres that showed the single TE mode property and which had the Brewster angle condition incorporated into their designs [7,9,10]. These values also allowed for all rings of holes in each case to have the same  $\Lambda_i$  with an integer number of holes.

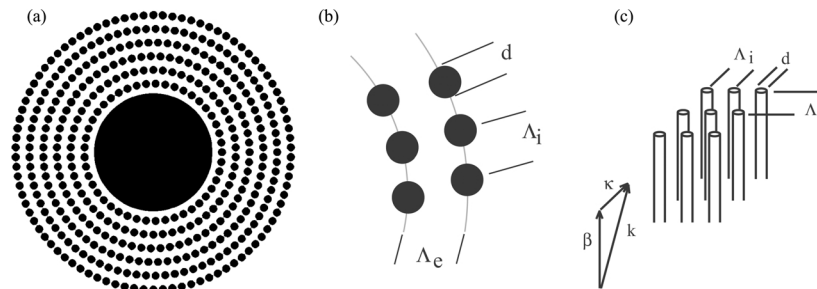


Fig. 1. Schematic of the ring-structured Bragg fibre (a) with some of the parameters indicated in (b). (c) The 2D lattice of holes that forms at large distances from the core. The wavevector is indicated by  $k$ , its longitudinal component by  $\beta$  and its transverse component by  $\kappa$ .

The Adjustable Boundary Condition method [13] was used for all numerical simulations of the fibre designs. It solves the vector form of Maxwell's equations using a Fourier decomposition in the azimuthal direction and a finite difference scheme in the radial direction. It accurately and efficiently calculates the complex effective index  $n_{eff}$  of each vector mode and the confinement loss (given by  $40\pi\text{Im}\{n_{eff}\}/[\lambda\ln(10)]$  in dB/m). The azimuthal Fourier decomposition requires only  $1/s$  of a structure with rotational symmetry  $s$  to be modelled. This contributed to the choice of the  $\Lambda_i$  values, which all result in a structure with some degree of rotational symmetry, increasing the speed of the calculations.

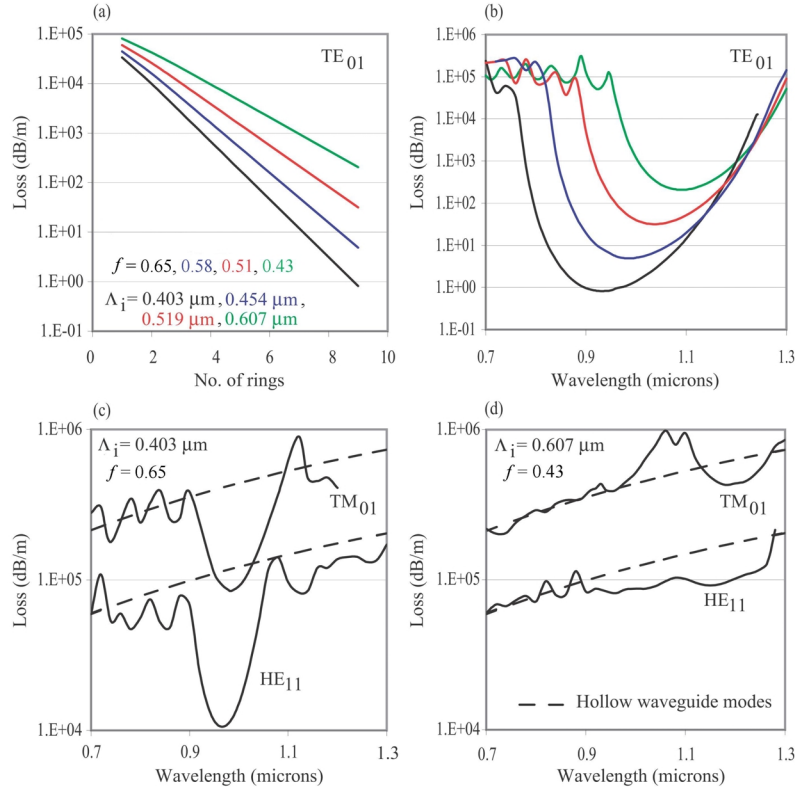


Fig. 2. (a) The loss of the  $TE_{01}$  mode (at the lowest loss wavelength) as a function of the number of rings for the different values of the air fraction. (b) The loss of the  $TE_{01}$  mode as a function of wavelength for the different values of  $f$  with 9 rings of holes, showing the loss and wavelength of lowest loss increasing with decreasing air fraction. (c) The loss of the  $HE_{11}$  and  $TM_{01}$  modes for  $f = 0.65$  ( $\Lambda_i = 0.403 \mu\text{m}$ ) with 9 rings of holes. (d) The loss of the  $HE_{11}$  and  $TM_{01}$  modes for  $f = 0.43$  ( $\Lambda_i = 0.607 \mu\text{m}$ ) with 9 rings of holes. The loss of the hollow waveguide  $HE_{11}$  and  $TM_{01}$  modes is also shown in (c) and (d) for comparison. The mechanism for isolating the  $TE_{01}$  mode is the large difference in the loss of the modes [9]. The  $HE_{11}$  mode has a loss of  $10^3$  to  $10^4$  times larger than that of the  $TE_{01}$  mode, depending on the value of  $\Lambda_i$ .

Increasing the number of rings for each value of  $f$  caused the loss of the  $TE_{01}$  mode to decrease as expected [see Fig. 2(a)]. As the air fraction in each ring is decreased the lowest loss wavelength shifts to the red and the loss increases [Fig. 2(b)]. This can be easily understood by considering the same effect in a 1D Bragg grating. Decreasing the air fraction increases the “average” refractive index of the low index layers of the grating. This reduces the index contrast and hence reduces the strength of the reflection, resulting in a higher confinement loss in the fibre. The Bragg condition for a layer of thickness  $\bar{d}$  and refractive index  $n$  is given by

$$\kappa \bar{d} = \sqrt{k^2(n^2 - \text{Re}\{n_{\text{eff}}\}^2)} \bar{d} = \pi / 2, \quad (1)$$

with  $\kappa$  the transverse wavenumber for light of free-space wavenumber  $k$ . It shows that increasing  $n$  requires the wavenumber to decrease, and thus the wavelength to increase. A small decrease in  $\text{Re}\{n_{\text{eff}}\}$  was observed as  $f$  was decreased (and hence  $n$  increased) which adds to this shift in wavelength. Figure 2(b) also shows that the wavelength range for which the loss decreases gets smaller with decreasing air fraction.

Some resonance features, although significantly smaller than for the TE<sub>01</sub> modes, were observed for the HE and TM polarisation modes for higher air fractions but were seen to decrease as the air fraction was reduced. As an example, the loss for the HE<sub>11</sub> and TM<sub>01</sub> modes for the highest and lowest air fractions used are shown in Figs. 2(c) and (d). The loss curve for a hollow waveguide (the hollow core on its own, with no additional structure) is also shown in those figures for comparison, and indicates that for the lower air fractions the rings of holes have very little effect on the HE<sub>11</sub> mode.

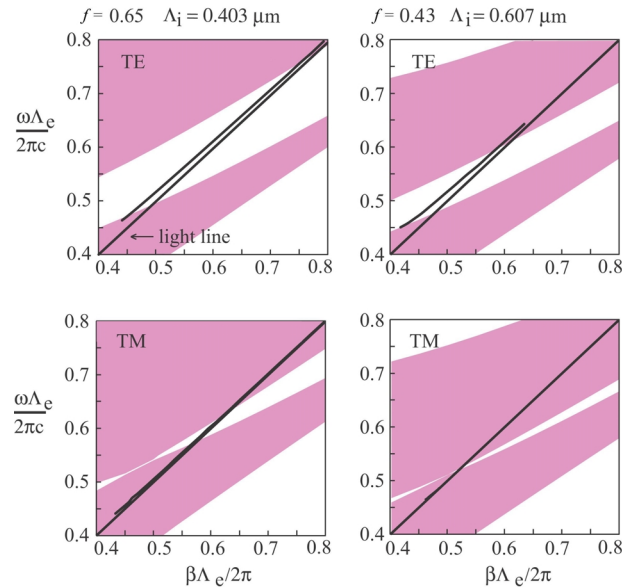


Fig. 3. Band diagrams for the highest and lowest air fraction of each ring of holes used for the TE and TM polarisations with the band gap regions denoted by white. The dispersion lines of the TE<sub>01</sub> modes are shown on the TE diagrams, and of the HE<sub>11</sub> mode on the TM diagrams (mostly indistinguishable from the light line on these graphs). The point where the TM band gap closes falls very close to the light line. This was achieved by incorporating the Brewster angle in these fibre designs [9].

These effects can be understood in terms of the band structure of the arrangements of holes in the cladding. The band diagrams for the highest and lowest air fraction are shown in Fig. 3 for the TE and TM polarisations. These were calculated for the 2D lattice of holes that forms at a large distance from the core [Fig. 1(c)] using standard Fourier decomposition methods [14]; details of these calculations can be found in [7]. For the TE case the dispersion line of the TE<sub>01</sub> mode is superimposed on the diagrams. It can be seen that the width of the band gap decreases with the air fraction. It is known for quarter-wave multilayer stacks that the width of the gap is related to the index contrast [15], a larger index contrast producing a wider band gap. In this case the lower air fraction results in a lower index contrast and hence a narrower band gap.

The dispersion line of the HE<sub>11</sub> mode has been shown on the TM diagram in Fig. 3 as the loss of the HE<sub>11</sub> mode is dominated by its TM component [16]. The TM gap is seen to close at one point – at that point the TM-polarised light is not reflected by the structure, similar to the Brewster angle effect. For the highest air fraction used here, the point where the band gap closes does not lie on the dispersion line of the HE<sub>11</sub> mode, and the mode crosses a region of the band gap where the gap is narrow, which is responsible for the small resonance features seen in Fig. 2(c). For the lowest  $f$  however, the HE<sub>11</sub> mode passes closer to the point where the band gap closes and so it effectively misses this primary gap entirely. This explains why

the loss curve resembles that of the hollow waveguide mode shown in Fig. 2(d) for the wavelength range considered.

The modelling results show the effects of reducing the air fraction of each ring of holes on the modes of the fibre. The most important result concerns the TE<sub>01</sub> mode, which shows an increase in the wavelength of lowest loss and the loss at that wavelength when the air fraction for each ring of holes is reduced. As more rings are added the low loss features become spectrally narrower and the decrease in loss slows with lower air fractions. Although the air fraction can be used to alter the properties of these fibres, it is not the only means through which the properties can be varied. Other parameters in the designs can be changed independently e.g. the core radius can be changed to alter the lowest loss wavelength and its loss [9,10]. For the most common microstructured fibre designs in which a triangular lattice of holes is used there are simple relations between the various parameters meaning that the fibre properties can be expressed in terms of dimensionless variables [1]. This cannot be done for the designs here because essentially all the parameters are independent.

The modelling results indicate that a homogenisation approximation to these designs is appropriate. The qualitative dependence on  $f$  of the loss, the wavelength of lowest loss and width of the band gaps was explained through considering a change in the “average” refractive index of each ring of holes. Also, the point where the TM band gap closes (Fig. 3) – the Brewster angle – depends on the air fraction. Thus it is clear that the lattice of holes approximates a multilayer stack, with the regions containing the holes acting as regions of (azimuthally) uniform refractive index, the index of which depends on the air fraction. If the lattice was not acting in such a way, all reflections in the structure could be considered as occurring off  $n = 1.49/1.0$  interfaces (matrix/hole), for which the Brewster angle would be fixed and not dependent on  $f$ . Previous work [7] showed the azimuthal orientation of the rings of holes with respect to each other, as well as the orientation of successive layers in the asymptotic 2D lattice (i.e. whether holes in adjacent layers line up) to be of no consequence.

### 3. Homogenisation approximations

Several approaches have been investigated to approximating structured fibres, similar to the ones here, as circularly symmetric structures. The main advantage gained by this is an increase in the speed and efficiency in which modes can be calculated, greatly simplifying the design and optimisation process. In an earlier paper [6] each ring of holes was replaced with a circularly symmetric index profile  $n(r)$  defined by the arithmetic mean in the azimuthal direction, given by

$$n(r) = \frac{1}{2\pi} \int_0^{2\pi} n(r, \phi) d\phi, \quad (2)$$

with  $n(r, \phi)$  the original profile of the structured fibre. For the solid core structure that guided by modified total internal reflection in [6] this approximation was able to reproduce the real parts of the  $n_{\text{eff}}$  with reasonable accuracy, but the imaginary parts were greatly underestimated. Similar homogenisation expansions have been proposed for solving the scalar wave equation for solid core structured fibres [17,18], which improve the agreement in the imaginary part, with agreement up to 7-20% reported in [17,19].

For a meaningful comparison to be made between the original structure and a homogenised approximation, the manner in which they are to be considered equivalent must first be determined. Each ring of holes has an associated reflection coefficient and an optical path length. The strength of the reflection will manifest itself in the loss of the modes, and the optical path length in determining the condition for Bragg reflection, and hence the lowest loss wavelength. Thus for two designs to be equivalent, they are to have the same lowest loss wavelength, and the same loss at that wavelength.

The first approach taken to finding a homogenised approximation was to use a conventional Bragg fibre, with low index layers of fixed refractive index (these fibres were initially intended to mimic conventional Bragg fibres). Each ring of holes was replaced by a homogeneous layer of constant refractive index  $n_{av}$  given by

$$n_{av} = \frac{\pi d}{4\Lambda_i} + \left(1 - \frac{\pi d}{4\Lambda_i}\right)n_1 = f + (1-f)n_1, \quad (3)$$

which is simply the arithmetic mean of the matrix refractive index  $n_1$  and the hole (air) refractive index, weighted by the air fraction of the ring of holes. The resulting index profile is shown in Fig. 4 for  $f = 0.65$ .

The results for the lowest loss wavelength and the loss at that wavelength for the index profiles created using Eq. (3) are presented in Fig. 5. The results from the structured fibres are also shown in Fig. 5, which is effectively a three-dimensional plot, the third parameter being

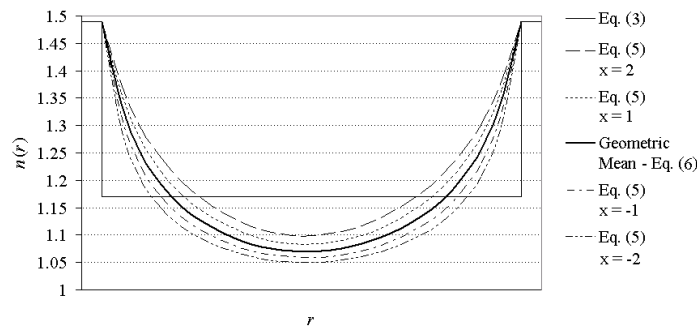


Fig. 4. The average refractive index profile  $n(r)$  obtained for one ring of holes with  $f = 0.65$  ( $\Lambda_i = 0.403 \mu\text{m}$ ) using the various methods discussed in the text.

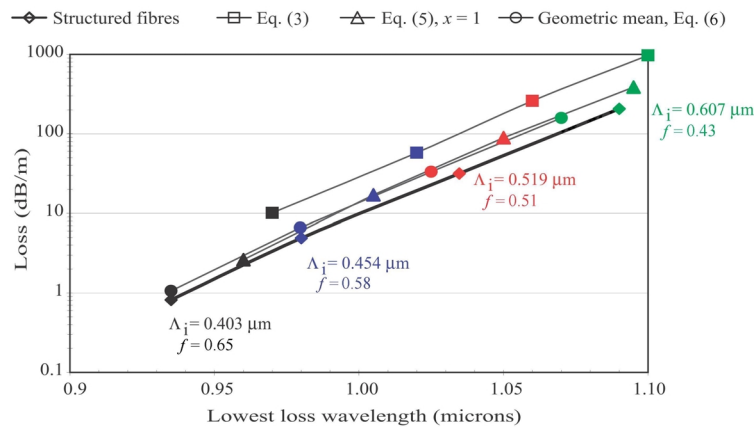


Fig. 5. Loss at the lowest loss wavelength for the ring-structured fibres and the various homogenisation approaches used. Only the curve for  $x = 1$  is plotted for Eq. (5) as it gave the best approximation compared to other values of  $x$  as described in the text.

the average index or  $f$  for the homogenised cases and  $\Lambda_i$  for the structured fibres, which varies along the curves. Figure 5 shows that the combination of loss and wavelength obtained from the ring-structured fibres cannot be reproduced using the approximation of a conventional

Bragg fibre. Although a wide range of averaging methods are available, as defined by the Voigt bounds [20]

$$n_{\text{av}} = \left[ \frac{\pi d}{4\Lambda_i} + \left( 1 - \frac{\pi d}{4\Lambda_i} \right) n_1^x \right]^{1/x} = \left[ f + (1-f)n_1^x \right]^{1/x}, \quad -2 \leq x \leq 2, \quad (4)$$

the only change in Fig. 5 would be the position of the labels along the curve, and not the curve itself [for  $x = 1$  this reproduces Eq. (3)].

The next iteration to this was to use a refractive index profile with radial dependence inside each ring as before [6], but with a slight modification to Eq. (2) to accommodate the range of averages allowed by Eq. (4)

$$n(r) = \left[ \frac{1}{2\pi} \int_0^{2\pi} n^x(r, \phi) d\phi \right]^{1/x}, \quad -2 \leq x \leq 2. \quad (5)$$

The results obtained from this approximation are also shown in Fig. 5 for  $x = 1$ , i.e. simply the arithmetic mean as given by Eq. (2);  $x = -1, -2$  and  $2$  were also tried but the agreement was not as good as for the arithmetic mean, and so these have not been included in Fig. 5. Although an improvement to Eq. (3), there is still disagreement between these results and those of the structured fibres. It was determined from the calculations that an appropriate value for  $n(r)$  would lie between those given by  $x = -1$  and  $1$ . This is true of the geometric mean, given by

$$n(r) = e^{\frac{1}{2\pi} \int_0^{2\pi} \ln[n(r, \phi)] d\phi}, \quad (6)$$

the results of which are also shown in Fig. 5. Using Eq. (6) gives the best approximation to the structured fibres at the shorter wavelengths that have the lowest loss, and hence are of most interest. The difference between the two varies from 0-2% for the wavelength of lowest loss and from 5-35% for the loss at those wavelengths (the loss values for the structured fibres used here are accurate to 2%). Second order corrections to  $n(r)$  are expected to be of the order of  $1/kr$  [18], and were found to make a contribution of less than a 1% change to the value of  $n(r)$ . The  $n(r)$  obtained using the various methods discussed are shown in Fig. 4 for one ring of holes for comparison.

Although no rigorous justification for why Eq. (6) results in the best approximation was sought in this work, it is noted that Maxwell's equation for the case of an optical fibre can be rewritten with the refractive index profile appearing only as  $\ln(n^2)$ , apart from terms containing the dependence of the wavenumber on refractive index [21]. A quick inspection shows that averaging this quantity reproduces Eq. (6).

#### 4. Surface modes

When the modal calculations presented in Fig. 2 were done over a larger wavelength range, interesting dispersion features were found, which are attributed to avoided crossings between modes supported in the solid part of the microstructure of the fibre, i.e. surface modes, and modes that would be supported by the hollow core in isolation. Surface modes in more conventional hollow core band gap fibres have been investigated recently [22] and appear to interfere with the band gap.

The avoided crossings occur between the surface modes, which have a  $\text{Re}\{n_{\text{eff}}\}$  that decreases rapidly with wavelength, and the modes the hollow core would support if the microstructure were to be removed, whose  $\text{Re}\{n_{\text{eff}}\}$  decreases slowly with wavelength, as shown in Fig. 6(a). When the  $\text{Re}\{n_{\text{eff}}\}$  of the surface modes falls below 1.0, the power of that

mode shifts from the solid parts of the fibre to the hollow core, and takes on the characteristics of a core mode, including the slowly varying  $\text{Re}\{n_{\text{eff}}\}$ . As the wavelength is increased further, the mode experiences a second avoided crossing with a surface mode and the  $\text{Re}\{n_{\text{eff}}\}$  begins to decrease rapidly with increasing wavelength once again. The power however remains largely in the core. The complex  $n_{\text{eff}}$  resulting from these interactions appear to obey the Kramers-Kronig relation, however this could not be verified to great accuracy as the  $n_{\text{eff}}$  would need to be known for a very large range of wavelengths.

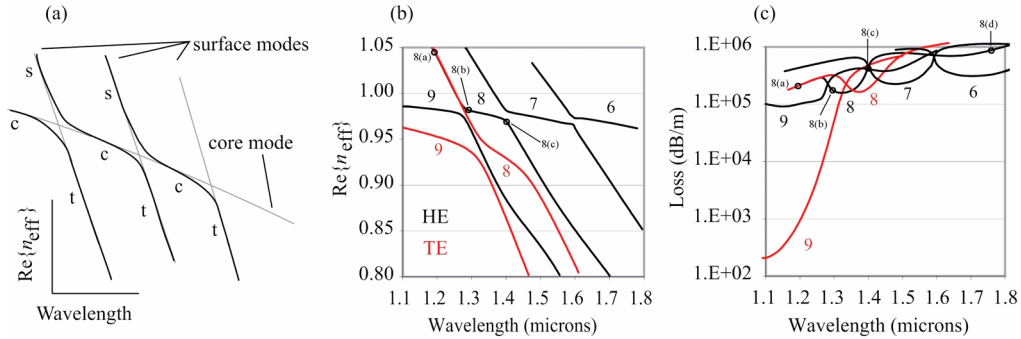


Fig. 6. (a) Schematic of  $\text{Re}\{n_{\text{eff}}\}$  as a function of wavelength indicating the effect of the avoided crossings and the surface mode “s”, core mode “c” and transition stage “t” of each mode. The  $\text{Re}\{n_{\text{eff}}\}$  (b) and loss (c) as a function of wavelength for  $f = 0.43$  ( $\Lambda_1 = 0.607 \mu\text{m}$ ) and HE polarisation from the middle of the primary band gap to longer wavelengths. The number of lobes in the intensity profile  $S_z$  of each mode is indicated. The intensity profile for the HE mode with 8 lobes is shown in Fig. 7 (for the wavelengths indicated) and in Fig. 8.

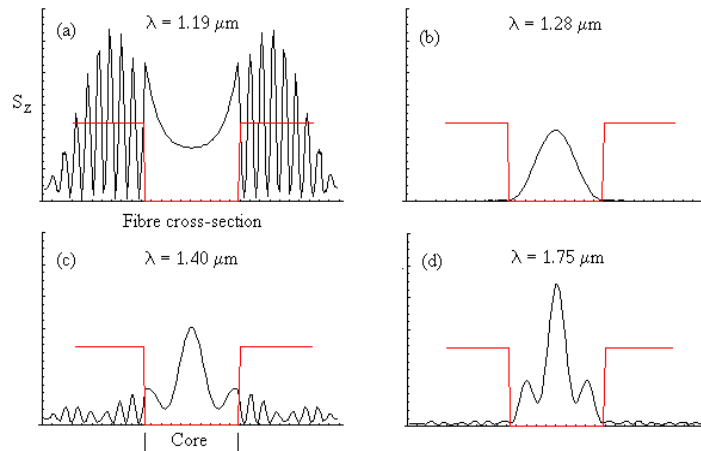


Fig. 7. The z-component of the Poynting vector  $S_z$  across the fibre for a HE polarisation mode in the surface mode stage (a), in the core mode stage (b), and in the transition stage (c and d).

Several interesting observations were made in the region of these avoided crossings. For each mode three wavelength regions can be defined: the short wavelength end where the  $\text{Re}\{n_{\text{eff}}\}$  decreases rapidly with wavelength is denoted as the surface mode stage, labeled s in Fig. 6(a), the middle wavelength range where the  $\text{Re}\{n_{\text{eff}}\}$  decreases slowly and the mode behaves like a core mode is denoted as the core mode stage (c) and the long wavelength end where the  $\text{Re}\{n_{\text{eff}}\}$  decreases rapidly again is denoted as the transition stage (t). All modes, when in the core mode stage can be labeled using notation derived from standard optical

fibres, and when the field components and properties thereof in the core are considered, the labeling can be done unambiguously. For the ring-structured fibre with 9 rings of holes and for  $f = 0.43$  ( $\Lambda_i = 0.607 \mu\text{m}$ ) some of these modes are shown in Fig. 6(b) and (c) for wavelengths longer than those of the primary band gap (the effects on the shorter wavelength side are nearly identical and so have been omitted from Fig. 6, although these can be seen in Fig. 2 for the lower  $f$  values). The dispersion properties arising from these avoided crossings would be qualitatively identical to those reported for conventional band gap fibres [22].

On either side of the primary band gap the core modes continue to appear the same, in that the intensity profile, i.e. the z-component of the Poynting vector  $S_z$ , remains largely unchanged in the core. The structure used here has 9 rings of holes and as a consequence  $S_z$  has an additional 9 lobes in the structured region, for wavelengths in the primary band gap. It was observed that all core modes at shorter wavelengths preserved this property, whilst core modes at longer wavelength did not. Once outside the primary band gap, every subsequent core mode has one less lobe in the structured region, decreasing to 8, 7 and 6 as seen in Fig. 6.

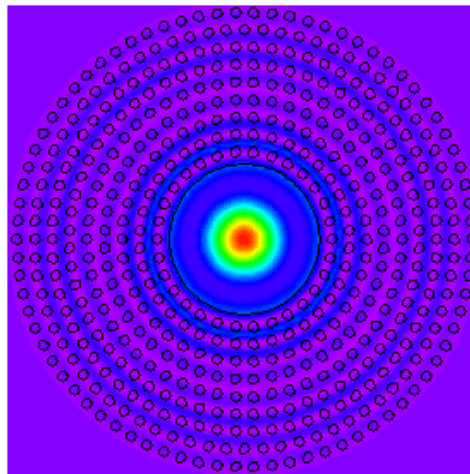


Fig. 8. The z-component of the Poynting vector  $S_z$  across the fibre for a HE polarisation mode as the wavelength is increased from 1.18 to 1.57  $\mu\text{m}$ , showing how the mode changes from a surface mode to a core mode and the transitions thereafter. Red indicates large intensities and violet low intensities. (animation – 1.61 MB)

When each mode was examined at wavelengths corresponding to its transition stage it was found that all underwent the same changes. The  $S_z$  of each mode initially appears as that of a core mode, with almost all of the power in the hollow core. A fraction of the power would then move out to the structured region and then back into the core, taking with it one lobe from the structured region to the core, as illustrated in Figs. 7 and 8. For a  $\text{HE}_{11}$  mode with 1 main lobe in the core and 8 lobes in the structured region when in its core mode stage, these transitions would result in the mode having 2 lobes in the core and 7 in the structure, then 3 in the core and 6 in the structure etc. A maximum of three transitions were observed as beyond that loss of the modes became too large for the numerical results to be reliable. For the fibres examined here, the surface modes seem to appear outside the band gap, where the loss of both core and surface modes is extremely high, making these modes largely inconsequential.

## 5. Conclusion

An analysis of a ring-structured Bragg fibre design that can support a single polarisation non-degenerate TE mode was presented. The air fraction of each ring of holes was decreased and

the loss and the wavelength of lowest loss were observed to both increase. The numerical results produced by modelling the ring-structured fibres were qualitatively explained by assuming that the rings of holes behaved as layers of azimuthally uniform refractive index, indicating that a homogenisation approach was appropriate. The index profile of such homogeneous layers would be determined by averaging the actual structure. It was found that best agreement for designs with the lowest loss was obtained when the geometrical average was used. This allows the ring-structured fibres to be modelled as circularly symmetric fibres, greatly increasing the speed of calculations and hence of further design or optimisation of these structures. A brief analysis of the surface modes supported by the fibre and their interactions with the hollow core was also presented.

Recent reports of the successful fabrication of a structured Bragg fibre [8] qualitatively similar to the ones analysed here (although single modedness was not reported) shows that the advantages these fibres offer are beginning to be recognised, and this work will contribute to the experimental realisation of a truly single mode circularly symmetric fibre.

### **Acknowledgments**

Nader Issa is acknowledged for providing the program used for the numerical simulation of the fibre modes and for useful discussions. The computer facilities at the Australian Partnership for Advanced Computing (APAC) and Sydney Vislab were used for this work.